

Electronic Supplementary Information

Experimental section

Chemicals and Materials: All reagents were analytical reagent grade and used as received without further purification. Nickel (II) nitrate hexahydrate ($\text{Ni}(\text{NO}_3)_2 \cdot 6\text{H}_2\text{O}$), urea ($\text{CH}_4\text{N}_2\text{O}$), Thioacetamide (TAA), Iron(III) chloride (FeCl_3), Sodium borohydride (NaBH_4), Polyvinylpyrrolidone ($(\text{C}_6\text{H}_9\text{NO})_n$) were purchased from Aladdin Ltd. (Shanghai, China). Nickel foam was obtained from Tianjin Aiwexin Chemical Technology Co. Ltd, with a thickness of 1 mm. The Ni foam was first cut into pieces at a size of 2 cm \times 4 cm. Then nickel foam plates (NF) were sequentially cleaned in 3 M HCl aqueous solution for 20 min, deionized water for 5 min and ethanol for 5 min via ultrasonic treatment, then dried in vacuum at 60°C.

Synthesis of Ni(oxy)hydroxides: 0.291g $\text{Ni}(\text{NO}_3)_2 \cdot 6\text{H}_2\text{O}$ and 0.6g urea were added in 40 mL ultrapure water. After vigorous magnetically stirred for 15 min, Transfer the formed clear solution to a 50 mL Teflon-lined stainless-steel autoclave, with a piece of cleaned NF (2 cm x 4 cm). Secondly, the Teflon-lined stainless-steel autoclave was sealed and maintained at 120 °C for 6 h, and then naturally cooled to room temperature. Thirdly, the NF covered with products was taken out and then washed with ultrapure water and ethanol several times before drying at 70 °C for 3 h

Synthesis of Ni_3S_2 NA/NF: TAA (0.23g) was dissolved in 40 mL ultrapure water, and this aqueous solution was moved to a Teflon-lined stainless-steel autoclave. The Ni(oxy)hydroxides were inserted into the above-mentioned reaction kettle and reacted at 120° C for 4 h. After cooling down to room temperature, the black product was taken out and then washed with ultrapure water and ethanol several times before drying at 70 °C for 3 h

Synthesis of Fe NPs-Ni₃S₂ NA/NF-10: 20 mM FeCl₃ 1 wt% PVP and 0.4 g NaBH₄ were dissolved in 40 mL ultrapure water at room temperature. The Ni₃S₂ NA/NF was inserted into the above solution, and then taken out after soaking for ten minutes. The dark brown product was taken out and then washed with ultrapure water and ethanol several times before drying at 70 °C for 3 h. In order to prevent Fe nanoparticles from being oxidized by air, the reduction of Fe (III) ions were carried out in nitrogen atmosphere and dried in vacuum. Other samples can be obtained by changing the reduction time.

Materials Characterization: The morphology of the materials was characterized using scanning electron microscopy (SEM FEI Quanta 250 FEG), transmission electron microscopy (TEM, Hitachi HT7700) and high-resolution TEM (HRTEM), which was recorded on a JEM-2100PLUS microscope with an accelerating voltage of 200kV. The element contents were tested by energy dispersive X-ray spectroscopy (EDS) on a FEI Quanta 250 FEG SEM. X-ray photoelectron spectroscopy (XPS, Thermo SCIENTIFIC ESCALAB 250Xi) was utilized to investigate the oxidation state and elemental composition. The crystal structure was analyzed by X-ray diffraction (XRD) with a Cu K α X-ray source ($\lambda = 1.540598 \text{ \AA}$). The contents of Fe and Ni were measured by inductively coupled plasma atomic emission spectroscopy (ICP-MS) using an Agilent 7700 instrument (USA).

Electrochemical measurements: All the electrochemical measurements were operated with a CHI660E electrochemical workstation using a three-electrode setup. Fe NPs-Ni₃S₂ NA/NF-10 was used as the working electrode. Graphite plate, and an Hg/HgO were used as the counter electrode and the reference electrode, respectively. The iR drops from the solution resistance during experiments were corrected. The polarization curves of OER performances were tested in 1 M KOH by linear sweep voltammetry (LSV) at a scan rate of 5 mV s⁻¹. The ECSA were investigated by double-layer capacitance (C_{dl}) in the

potential range from 0.92 to 1.02V vs. RHE. The electrochemical impedance spectroscopy (EIS) at 0.31 V (vs. RHE) was collected with frequency range from 0.1 Hz to 100 KHz and alternating voltage of 5 mV. The potentials reported in this work were calibrated to RHE other than especially explained, using the following equation: $E(\text{RHE}) = E(\text{Hg/HgO}) + (0.098 + 0.059 \text{ pH}) \text{ V}$. The TOF was calculated by the equation: $\text{TOF} = (J \times A) / (4 \times F \times m)$, where J represents the current density (A cm^{-2}) at an overpotential of 300mV, A and m represent the area of the electrode and the number of moles of the active materials.

FE determination: The FE was calculated by comparing the amount of measured O_2 generated by anodal electrolysis with calculated O_2 (assuming 100% FE). GC analysis was carried out on GC-2014C (Shimadzu Co.) with thermal conductivity detector and nitrogen carrier gas. Pressure data during electrolysis were recorded using a CEM DT-8890 Differential Air Pressure Gauge Manometer Data Logger Meter Tester with a sampling interval of 1 point per second.

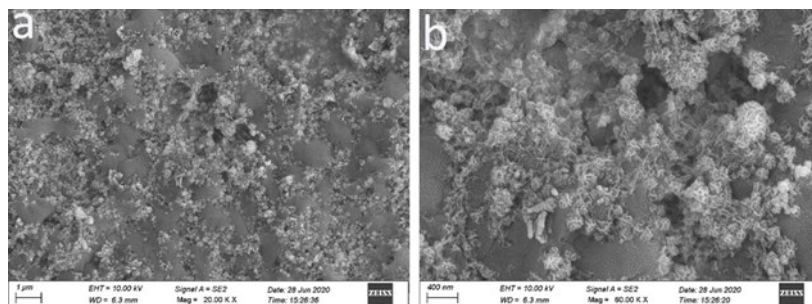


Fig. S1. SEM image of Fe NPs- Ni_3S_2 NA/NF.

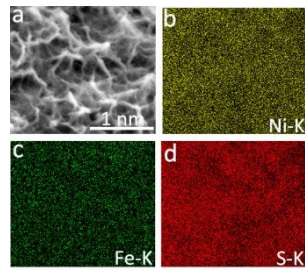
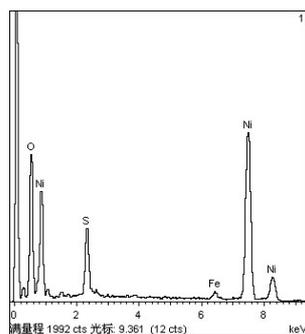


Fig.S2. EDX elemental mapping images of Ni, Fe and S for Fe NPs-Ni₃S₂ NA/NF-10.



Element	Wt%	At%
O K	0.62	58.05
S K	0.23	6.08
Fe K	0.19	0.68
Ni K	0.63	35.19

Fig. S3. Content of each element

Table. S1. ICP-MS of Fe NPs-Ni₂S₃ NA/NF-10.

Sample	Ni (Wt %)	Fe (Wt %)
Fe NPs-Ni ₃ S ₂ NA/NF-10 (Initial)	4.2%	0.52%
Fe NPs-Ni ₃ S ₂ NA/NF-10 (After 1000 cycles)	4.0%	0.49%

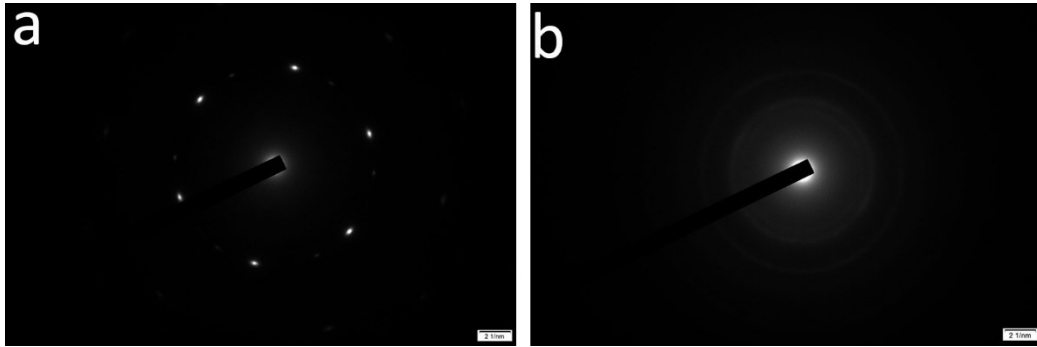


Fig. S4. (a) SAED of Ni_3S_2 NA/NF (d) SAED of Fe NPs- Ni_3S_2 NA/NF-10.

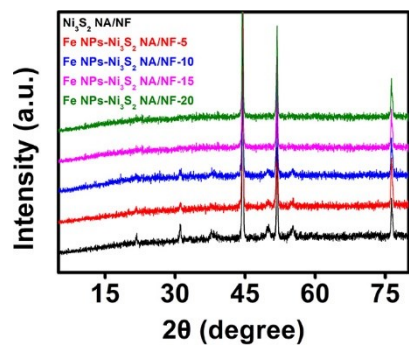


Fig. S5. XRD patterns of Ni₃S₂ NA/NF, Fe NPs-Ni₃S₂ NA/NF-5, Fe NPs-Ni₃S₂ NA/NF-10, Fe NPs-Ni₃S₂ NA/NF-15 and Fe NPs-Ni₃S₂ NA/NF-20.

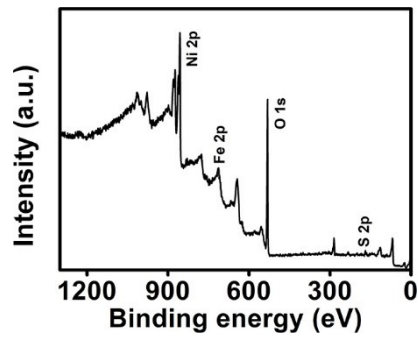


Fig. S6. XPS survey spectrum for Fe NPs-Ni₃S₂ NA/NF-10.

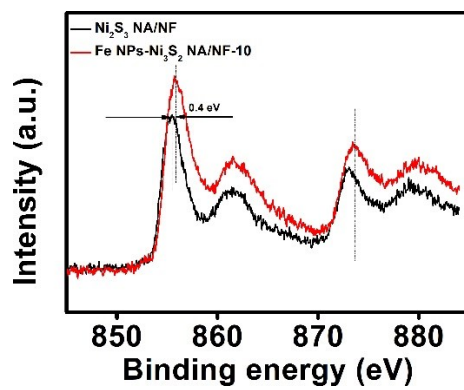


Fig. S7. XPS spectra in the Ni 2p regions for Fe NPs- Ni_3S_2 NA/NF-10.

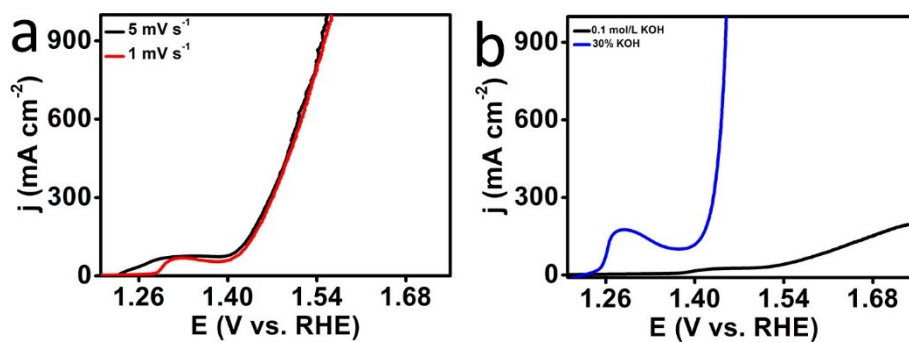


Fig. S8. (a) Linear sweep voltammetry of Fe NPs-Ni₃S₂ NA/NF-10 with a scan rate of 1 mV s⁻¹ and 5 mV s⁻¹. (b) LSV curves for Fe NPs-Ni₃S₂ NA/NF-10 in 0.1 M KOH and 30 wt% KOH.

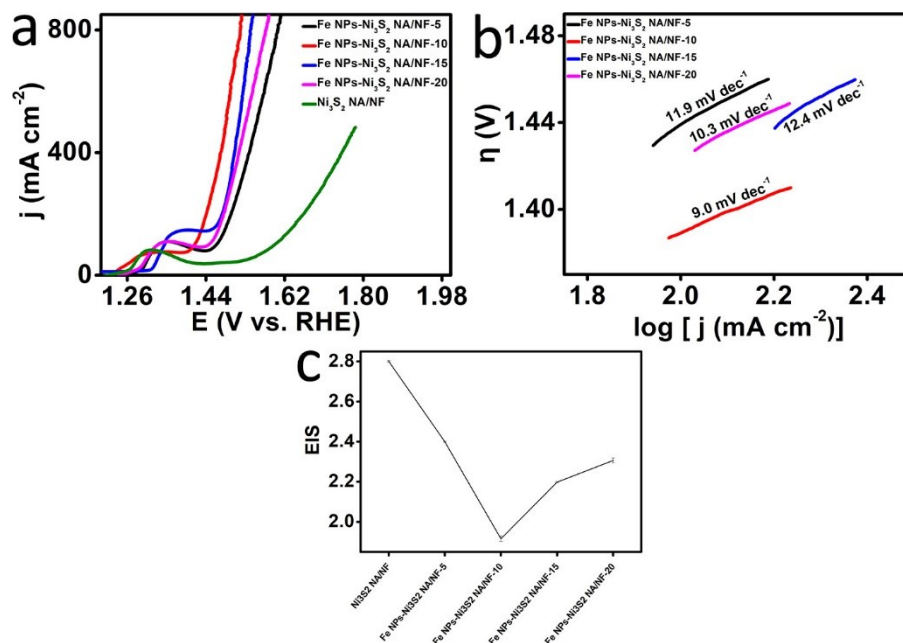


Fig. S9. (a) LSV curves of Ni₃S₂ NA/NF, Fe NPs-Ni₃S₂ NA/NF-5, Fe NPs-Ni₃S₂ NA/NF-10, Fe NPs-Ni₃S₂ NA/NF-15 and Fe NPs-Ni₃S₂ NA/NF-20 with a scan rate of 5 mV s⁻¹ for water oxidation. (b) Tafel plots for Ni₃S₂ NA/NF, Fe NPs-Ni₃S₂ NA/NF-5, Fe NPs-Ni₃S₂ NA/NF-10, Fe NPs-Ni₃S₂ NA/NF-15 and Fe NPs-Ni₃S₂ NA/NF-20. (c) The electrochemical impedance spectroscopy (EIS) for Ni₃S₂ NA/NF, Fe NPs-Ni₃S₂ NA/NF-5, Fe NPs-Ni₃S₂ NA/NF-10, Fe NPs-Ni₃S₂ NA/NF-15 and Fe NPs-Ni₃S₂ NA/NF-20.

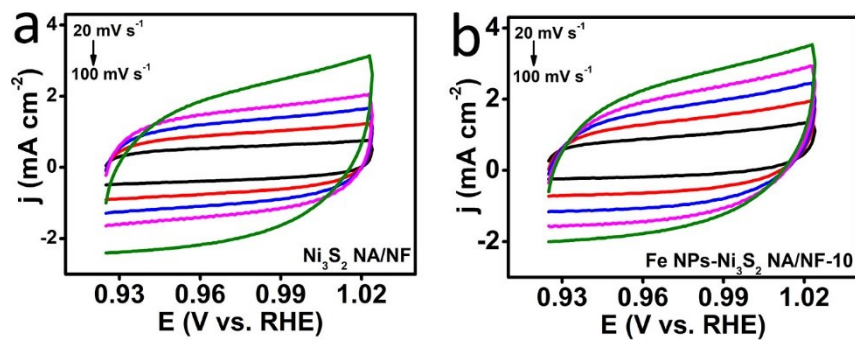


Fig. S10. CVs of (a) Ni_3S_2 NA/NF, (b) Fe NPs- Ni_3S_2 NA/NF-10 with various scan rates.

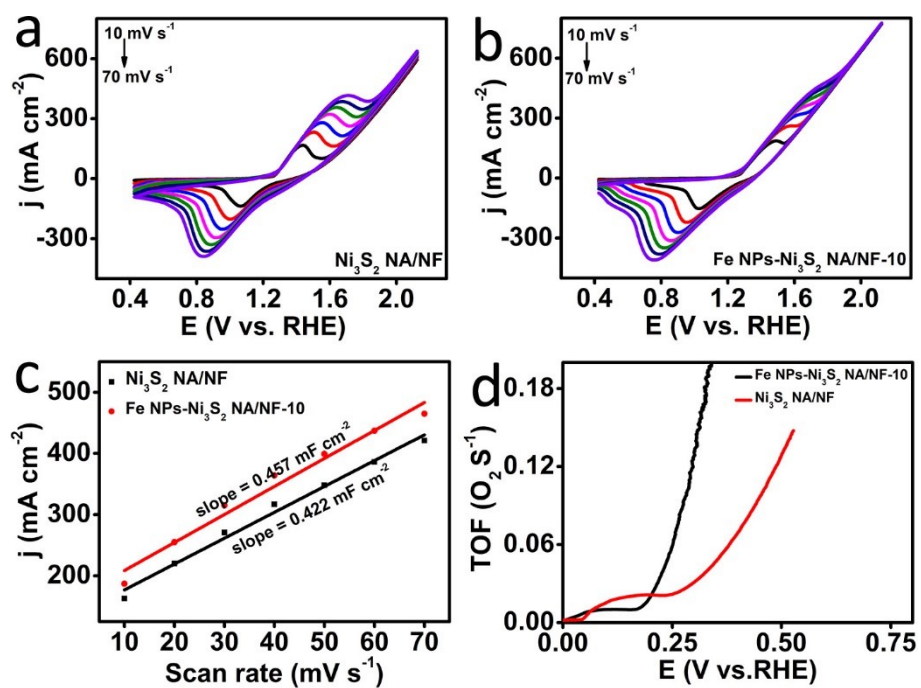


Fig.S11. (a) CVs for Ni_3S_2 NA/NF in the faradaic capacitance current range at scan rates from 10 to 70 mV s^{-1} in 1.0 M KOH at room temperature. (b) CVs for $\text{Fe NPs-Ni}_3\text{S}_2$ NA/NF-10 in the faradaic capacitance current range at scan rates from 10 to 70 mV s^{-1} in 1.0 M KOH at room temperature. (c) Oxidation peak current versus scan rate plot for Ni_3S_2 NA/NF and $\text{Fe NPs-Ni}_3\text{S}_2$ NA/NF-10. (d) Plot of the TOF of Ni_3S_2 NA/NF and $\text{Fe NPs-Ni}_3\text{S}_2$ NA/NF-10 as a function of the overpotential.

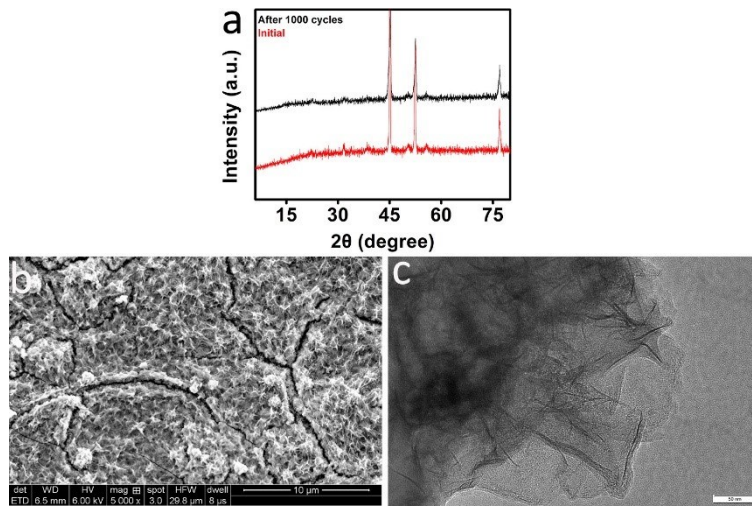


Fig. S12. (a) XRD patterns of Fe NPs- Ni_3S_2 NA/NF-10 after 1000 cycles. SEM image of Fe NPs- Ni_3S_2 NA/NF-10 after 1000 cycles. TEM image of Fe NPs- Ni_3S_2 NA/NF-10 after after 1000 cycles.

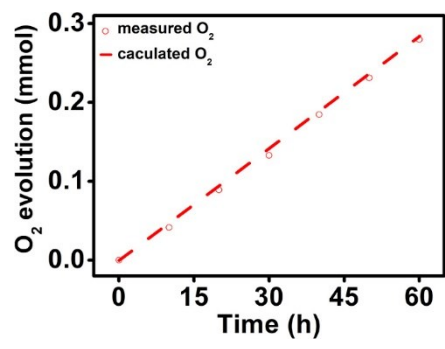


Fig. S13. The amount of O₂ theoretically calculated and experimentally measured versus time for oxygen evolution of Fe NPs-Ni₃S₂ NA/NF-10.

Table S2. The comparison of catalytic performances for OER in 1 M KOH between Fe NPs-Ni₃S₂ NA/NF-10 and other sulfide materials reported in the literature.

	j (mA cm⁻²)	η(mV)	Electrolyte	Reference
Fe NPs-Ni ₃ S ₂ NA/NF-10	150	206	1.0 M KOH	This work
Fe _{17.5%} -Ni ₃ S ₂ /NF	10/20/100	214/222/249	1.0 M KOH	1
Fe-Ni ₃ S ₂ /FeNi	10/20	282/320	1.0 M KOH	2
Fe _{0.1} -NiS ₂ NA/Ti	100	231	1.0 M KOH	3
Fe _{11.8%} -Ni ₃ S ₂ /NF	100	253	1.0 M KOH	4
MoO _x /Ni ₃ S ₂ /NF	100	310	1.0 M KOH	5
200-SMN/NF (Mo doped Ni ₃ S ₂)	100	400	1.0 M KOH	6
Ni _x Co _{3-x} S ₄ /Ni ₃ S ₂ /NF	100	320	1.0 M KOH	7
MoS ₂ /Ni ₃ S ₂ heterostructures	10/100	218/290	1.0 M KOH	8
High-Index Faceted Ni ₃ S ₂ /NF	10/20	260/280	1.0 M KOH	9
N-Ni ₃ S ₂ /NF	100	340	1.0 M KOH	10
MoS ₂ -Ni ₃ S ₂ HNRs/NF	10/100	249/341	1.0 M KOH	11
NiS/NF	100	370	1.0 M KOH	12
FNHNS/NF	10/20/100	290/320/445	1.0 M KOH	13
Ni/NiS	20/100	320/390	1.0 M KOH	14
FeNiS ₂ NSs	10	310	1.0 M KOH	15
NiFeS-1/NF	100	230	1.0 M KOH	16
Zn-Ni ₃ S ₂ /NF	100	300	1.0 M KOH	17
Ni _{0.9} Fe _{0.1} PS ₃	20	329	1.0 M KOH	18
NiCo ₂ S ₄ NA/CC	20/100	280/340	1.0 M KOH	19
NiCo ₂ S ₄ NW/NF	10	260	1.0 M KOH	20

Table S3. Comparison of TOF value for Fe NPs-Ni₃S₂ NA/NF-10 min with other non-noble-metal OER electrocatalysts in alkaline media.

Catalyst	j (mA cm ⁻²)	TOF (mol O ₂ s ⁻¹)	Electrolyte	Reference
Fe NPs-Ni ₃ S ₂ NA/NF-10	300	0.12	1.0 M KOH	This work
NiCo ₂ O ₄ @Ni- Co-B/CC	500	0.019	1.0 M KOH	21
Ni ₃ S ₂ @G	220	0.035	1.0 M KOH	22
Co ₉ S ₈	285	0.0268	1.0 M KOH	23
NiFe	400	0.075	1.0 M KOH	24

1. G. Zhang, Y. Feng, W. Lu, D. He, C. Wang, Y. Li and F. Cao, *ACS Catal.*, 2018, **8**, 5431-5441.
2. C. Z. Yuan, Z. T. Sun, Y. F. Jiang, Z. K. Yang, N. Jiang, Z. W. Zhao, U. Y. Qazi, W. H. Zhang, A. W. Xu, *Small*, 2017, **13**, 1604161.
3. N. Yang, C. Tang, K. Y. Wang, G. Du, A. M. Asiri, X. P. Sun, *Nano Res.*, 2016, **9**, 3346-3354
4. N. Y. Cheng, Q. Liu, A. M. Asiri, W. Xing, X. P. Sun, *J. Mater. Chem. A.*, 2015, **3**, 23207-23212.
5. Y. Wu, G. D. Li, Y. Liu, L. Yang, X. Lian, T. Asefa, X. Zou, *Adv. Funct. Mater.*, 2016, **26**, 4839-4847.
6. Z. Cui, Y. C. Ge, H. Chu, R. Baines, P. Dong, J. H. Tang, Y. Yang, P. M. Ajayan, M. X. Ye, J. F. Shen, *J. Mater. Chem. A.*, 2017, **5**, 1595-1602.
7. Y. Wu, Y. Liu, G. D. Li, X. Zou, X. Lian, D. Wang, L. Sun, T. Asefa, X. Zou, *Nano Energy.*, 2017, **35**, 161-170.
8. J. Zhang, T. Wang, D. Pohl, B. Rellinghaus, R. Dong, S. Liu, X. Zhuang, X. Feng, *Angew. Chem. Int. Ed.*, 2016, **55**, 6702-6707.
9. L. L. Feng, G. Yu, Y. Wu, G. D. Li, H. Li, Y. Sun, T. Asefa, W. Chen, X. Zou, *J. Am. Chem. Soc.*, 2015, **137**, 14023-14026.
10. P. Chen, T. Zhou, M. Zhang, Y. Tong, C. Zhong, N. Zhang, L. Zhang, C. Wu, Y. Xie, *Adv. Mater.*, 2017, **29**, 1701584.
11. Y. Yang, K. Zhang, H. Lin, X. Li, H. C. Chan, L. Yang, Q. Gao, *ACS Catal.*, 2017, **7**, 2357-2366.
12. W. Zhu, X. Yue, W. Zhang, S. Yu, Y. Zhang, J. Wang, J. Wang, *Chem. Commun.*, 2016, **52**, 1486-1489.
13. J. Liu, Y. Yang, B. Ni, H. Li, X. Wang, *Small*, 2017, **13**, 1602637.
14. G. F. Chen, T. Y. Ma, Z. Q. Liu, N. Li, Y. Z. Su, K. Davey, S. Z. Qiao, *Adv. Funct. Mater.*, 2016, **26**, 3314-3323.
15. J. Jiang, S. Lu, H. Gao, X. Zhang, H. Q. Yu, *Nano Energy*, 2016, **27**, 526-534.
16. P. Ganesan, A. Sivanantham, S. Shanmugam, *J. Mater. Chem. A.*, 2016, **4**, 16394-16402.

17. Q. Liu, L. S Xie, Z. Liu, G. Du, A. M. Asiri, X. P. Sun, *Chem. Commun.*, 2017, **53**, 12446-12449.
18. B. Song, K. Li, Y. Yin, T. Wu, L. Dang, M. Cabán-Acevedo, J. Han, T. Gao, X. Wang, Z. Zhang, J. R. Schmidt, P. Xu, S. Jin, *ACS Catal.*, 2017, **7**, 8549-8557.
19. D. Liu, Q. Lu, Y. Luo, X. Sun, A. M. Asiri, *Nanoscale*, 2015, **7**, 15122-15126.
20. A. Sivanantham, P. Ganesan, S. Shanmugam, *Adv. Funct. Mater.*, 2016, **26**, 4661-4672.
21. X. Ji, X. Ren, S. Hao, F. Xie, F. Qu, G. Du, A. Asirif and X. Sun, *Inorg. Chem. Front.*, 2017, **4**, 1546–1550.
22. J. Yu, Y. Du, Q. Li, L. Zhen, V. Dravid, J. Wu and C. Xu, *Appl. Surf. Sci.*, 2019, **465**, 772–779.
23. X. Feng, Q. Jiao, T. Liu, Q. Li, M. Yin, Y. Zhao, H. Li, C. Feng and W. Zhou, *ACS Sustainable Chem. Eng.*, 2018, **6**, 1863–1871.
24. X. Lu and C. Zhao, *Nat. Commun.*, 2015, **6**, 6616.